A flexible loop as a functional element in the catalytic mechanism of nucleoside hydrolase from Trypanosoma vivax

Vandemeulebroucke, An; De Vos, Stefan; Van Holsbeke, Els; Steyaert, Jan; Versees, Wim

Published in:
Journal of Biological Chemistry

Publication date:
2008

Document Version:
Final published version

THE JOURNAL OF BIOLOGICAL CHEMISTRY VOL. 283, NO. 32, pp. 22272–22282, August 8, 2008

A Flexible Loop as a Functional Element in the Catalytic Mechanism of Nucleoside Hydrolase from *Trypanosoma vivax*[*]

Received for publication, May 14, 2008 Published, JBC Papers in Press, June 2, 2008, DOI 10.1074/jbc.M803705200

An Vandemeulebroucke[1], **Stefan De Vos, Els Van Holsbeke, Jan Steyaert**[2], **and Wim Versées**[3]

From the Departments of Ultrastructure and Molecular and Cellular Interactions, Vrije Universiteit Brussel (VIB), Pleinlaan 2, Brussels 1050, Belgium

The nucleoside hydrolase of *Trypanosoma vivax* hydrolyzes the *N*-glycosidic bond of purine nucleosides. Structural and kinetic studies on this enzyme have suggested a catalytic role for a flexible loop in the vicinity of the active sites. Here we present the analysis of the role of this flexible loop via the combination of a proline scan of the loop, loop deletion mutagenesis, steady state and pre-steady state analysis, and x-ray crystallography. Our analysis reveals that this loop has an important role in leaving group activation and product release. The catalytic role involves the entire loop and could only be perturbed by deletion of the entire loop and not by single site mutagenesis. We present evidence that the loop closes over the active site during catalysis, thereby ordering a water channel that is involved in leaving group activation. Once chemistry has taken place, the loop dynamics determine the rate of product release.

The importance of conformational changes in enzyme catalysis has long been appreciated. These changes are thought to fulfill a number of roles in catalysis: enhanced binding of substrate, correct orientation of catalytic groups, removal of water from the active site, and trapping of intermediates. Loop motion is classified as an enzyme conformational change, where flexible surface loops move to different conformations (1).

Flexible loops are also a common feature of the family of nucleoside hydrolases (EC 3.2.2.1) (2). All structures of the nucleoside hydrolases determined until now show two flexible loops in the vicinity of the active sites, which undergo substantial conformational changes upon association of substrates and inhibitors (2). Nucleoside hydrolases (NHs)[4] catalyze the hydrolysis of the *N*-glycosidic bond of nucleosides, forming ribose and the corresponding base (Fig. 1) (2). It has been shown that the NH-catalyzed hydrolysis proceeds via a highly dissociative S_N2-type mechanism with an oxocarbenium ion-like transition state (3, 4). A general catalytic mechanism based on three strategies has been proposed: activation of the nucleophilic water molecule, steric and electrostatic stabilization of the oxocarbenium ion, and leaving group (LG) activation by protonation or hydrogen bonding (2).

The purine-specific nucleoside hydrolase of *Trypanosoma vivax* (*Tv*NH) has been very well characterized kinetically and structurally. This allowed us to put forward a detailed catalytic mechanism to accomplish these strategies. An aspartate (Asp^{10}) in the ribose binding pocket acts as a general base to activate the nucleophile water (5). The oxocarbenium ion is stabilized through interactions between the enzyme and all of the hydroxyl groups (6). The third catalytic strategy, LG activation, was thought to be accomplished by a Brönsted acid, which protonates nitrogen-7 (N-7) of the purine base (2, 7–9). However, in *Tv*NH, no obvious proton donor was found. Here, the LG of the substrate is stacked between the two indole side chains of Trp^{83} and Trp^{260} (Fig. 2*A*). A novel catalytic mechanism in which the arene-arene stacking interaction between Trp^{260} and the purine LG substantially increases the latter's pK_a at N-7, thus facilitating its protonation by solvent, has been proposed (10). Substrate-assisted catalysis was suggested as an additional mechanism for leaving group activation via hydrogen bond formation between the O-5′ of the ribose moiety and the C-8 hydrogen of the purine leaving group (11) (Fig. 2*A*).

In the unliganded structures of *Tv*NH, two flexible loops at opposite sides of the active site, called loop 1 and 2, are present with low or no associated electron density. Loop 1 is located at the C-terminal end of β3 and comprises residues 75–85; loop 2 is situated at the C-terminal end of a long α-helix and comprises residues 244–258. Binding of the ground state inhibitor 3-deaza-adenosine to wild type *Tv*NH as well as binding of the substrate inosine to a slow mutant of this enzyme orders loop 1 (6). Ordering of loop 1 brings Trp^{83} into a parallel stacking interaction with the nucleobase. Recently, we also solved the structure of *Tv*NH in complex with the transition state analogue inhibitor immucillin-H (ImmH) (12). In this structure, loop 1 and loop 2 are ordered. Loop 2 folds over the active site, establishing a previously unobserved closed conformation of the active site of *Tv*NH (Fig. 2*B*). Furthermore, the ordered loop 1 of one subunit of the dimeric protein interacts with the ordered loop 2 of the other subunit, and *vice versa*. A mechanism of loop

[*] The costs of publication of this article were defrayed in part by the payment of page charges. This article must therefore be hereby marked "*advertisement*" in accordance with 18 U.S.C. Section 1734 solely to indicate this fact.

The atomic coordinates and structure factors (code 3B9G) have been deposited in the Protein Data Bank, Research Collaboratory for Structural Bioinformatics, Rutgers University, New Brunswick, NJ (http://www.rcsb.org/).

[1] Supported by a grant from the Institute for the Promotion of Innovation through Science and Technology in Flanders (IWT-Vlaanderen).

[2] To whom correspondence should be addressed. Tel.: 3226291931; Fax: 3226291963; E-mail: jan.steyaert@vub.ac.be.

[3] Supported by a grant from FWO-Vlaanderen.

[4] The abbreviations used are: NH, nucleoside hydrolase; LG, leaving group; *Tv*NH, nucleoside hydrolase from *T. vivax*; wt*Tv*NH, wild type *Tv*NH; ImmH, immucillin H or (1*S*)-1-(9-deazaadenin-9-yl)-1,4-dideoxy-1,4-imino-D-ribitol; 3G*Tv*NH, loop deletion mutant of *Tv*NH; 2apr, 2-aminopurine riboside; 7mguo, 7-methyl guanosine.

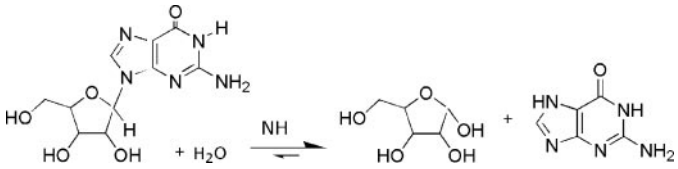

FIGURE 1. **The nucleoside hydrolase-catalyzed hydrolysis reaction of a nucleoside, exemplified by guanosine.**

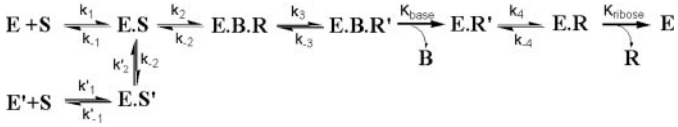

SCHEME 1. **Kinetic model for wild type *Tv*NH.** *E*, enzyme; *S*, substrate; *B*, base; *R*, ribose.

closure has been proposed that links binding of the substrate's 2′-OH group via a conformational change of Asp^{14} and Trp^{242} to loop closure. The Trp^{260} side chain approaches N-7 of the LG by 0.6 Å in the transition state structure, corroborating its central role in leaving group activation. In this closed conformation, the N-7 of the purine does not interact with any amino acid residue but is connected to bulk solvent by a network of highly ordered water molecules. This water channel, possibly aided by the polar residues of loop 2 lining it (*e.g.* Arg^{252} and Asp^{255}), can act as a proton relay system shuttling protons directly to the high pK_a N-7.

All structural findings suggest an important catalytic role for the flexible loop residues. In this paper, we set out to test this hypothesis by mutagenesis and x-ray crystallography. However, interpretations of effects of mutagenesis on *Tv*NH activity based on steady-state parameters are potentially misleading due to its complex kinetic mechanism. Indeed, a detailed kinetic analysis of *Tv*NH has allowed the assignment of transients corresponding to binding, chemistry, base release, and ribose release (13). Together, this pre-steady state characterization has led to the development of a detailed kinetic mechanism (Scheme 1). The kinetic model is based on fast chemistry (*N*-glycosidic bond cleavage), followed by an ordered product release. Dissociation of the base precedes the slow overall rate-limiting ribose release. Binding experiments have shown that ribose release in itself is a two-step process consisting of a rate-limiting isomerization of a tightly bound enzyme-ribose complex to a loosely bound complex from which ribose can easily dissociate. The development of this model permitted us to examine the effects of mutagenesis on these individual processes.

The here reported analysis of the catalytic role of the flexible loop 2 in the mechanism of *Tv*NH suggests an important function in LG activation. The loop presumably closes over the active site during catalysis, thereby ordering a water channel that is involved in LG activation. Once chemistry has taken place, the loop dynamics determine the rate of product release.

MATERIALS AND METHODS

Production of the Mutant TvNHs—The *Tv*NH open reading frame was cloned into the BamHI-HindIII restriction sites of the pQE-30 plasmid (Qiagen) and used as the template for all *in vitro* mutagenic studies. The individual mutations in the loop region (proline scan) were created using the QuikChange™ site-directed mutagenesis kit according to the protocol supplied by the manufacturer. The loop deletion mutant (3G*Tv*NH) was created using a primer extension overlap PCR. A forward primer and a complementary reverse primer containing the codons for three glycine residues replacing the 13 loop residues were used together with a general reverse and forward primer for the pQE-30 plasmid to generate the 3′ and 5′ fragments of the mutated open reading frame. A second PCR with the general primers was used to link both fragments together. This PCR product was recloned in the pQE-30 plasmid using the BamHI and HindIII restriction sites.

Expression and Purification—Expression and purification of the wild type and mutant *Tv*NHs were performed as described previously (5). *Escherichia coli* cells (WK6) containing the *Tv*NH open reading frame cloned in the pQE-30 expression vector were used to express the protein. The presence of an N-terminal His_6 tag allowed for a two-step purification scheme, consisting of an Ni^{2+}-nitrilotriacetic acid affinity chromatography step (Qiagen), followed by a gel filtration on a Superdex-75 column (Amersham Biosciences).

General Procedures for Kinetic Analysis—The concentrations of nucleosides and purine stock solutions were determined using the following extinction coefficients (14): ϵ_{253} = 13.6 mM^{-1} cm^{-1} for guanosine; ϵ_{258} = 8.5 mM^{-1} cm^{-1} for 7-methylguanosine; ϵ_{260} = 1 mM^{-1} cm^{-1} for 2-aminopurine; and $\epsilon_{248.5}$ = 12.3 mM^{-1} cm^{-1} for inosine. Nucleosides and purine solutions were freshly made in deionized water. Once thawed, enzyme stocks were kept at 4 °C and used over a period of several days but never refrozen to avoid activity loss. All kinetic measurements were performed in 50 mM potassium phosphate buffers, adjusted with NaCl to a constant ionic strength of 200 mM.

Steady State Kinetics—Initial rate kinetic measurements were carried out at 25 °C and pH 7.0. Product formation was analyzed spectrophotometrically using the difference in absorption between the nucleoside and the base. The $\Delta\epsilon$ values (mM^{-1} cm^{-1}) used were as follows: guanosine, −4.0 at 260 nm; 7-methylguanosine, −4.4 at 258 nm; and 2-aminopurine riboside, −2.29 at 250 nm. All data were fitted to the Michaelis-Menten equation using the program Origin (Microcal). Kinetic parameters were calculated per active site.

To determine the inhibition constants for the ImmH, we analyzed the influence of ImmH on the steady state parameters of inosine hydrolysis. Xanthine oxidase was used in a coupled assay to monitor inosine hydrolysis at 25 °C and pH 7.5 (optimal pH of xanthine oxidase). By adding xanthine oxidase, the reaction product hypoxanthine is oxidized to uric acid, which can be monitored spectrophotometrically at 293 nm (ϵ_{293} uric acid, 12.9 mM^{-1} cm^{-1}). Reactions were started by adding the NH enzyme to the reaction mixture containing 500 μM inosine, 120 milliunits of xanthine oxidase/ml, and variable concentrations of inhibitor. Inhibition data were analyzed using the linearized plots of Dixon.

Solvent Isotope Effect Measurements—The solvent isotope effect measurements were performed as described previously (15). The pD of the buffer made up in deuterium oxide was adjusted with DCl, and the pD meter reading was corrected using the relation, pD = (meter reading) + 0.4. The buffers

were used on the day of making and consisted of 50 mM phosphate buffers at 0.2 M ionic strength with NaCl and pL = 7.0. The enzymes were not exchanged into D_2O-containing buffer, but the final concentration of H_2O was <0.001%. No change in enzyme activity was observed in D_2O-containing buffer after 3 h of incubation on ice. Guanosine was used as a substrate for the initial rate kinetic measurements at 25 °C.

Stopped Flow Methods—Stopped flow analysis was performed on an Applied Photophysics model SX18.MV stopped flow spectrofluorimeter fitted with a xenon lamp. All experiments were performed at 5 °C and pH 7.0. All reported concentrations correspond to final concentrations in the reaction chamber after mixing. Progress curves were averaged (generally 10–14 shots) and corrected for background signal changes by subtracting the averaged progress curve for a sample containing substrate only (for absorption measurements) or enzyme only (for fluorescence measurements).

Multiple turnovers of substrate (excess of substrate over enzyme) were analyzed by stopped flow absorbance using the difference in absorption between the nucleoside and the base. For these absorption measurements, the photomultiplier voltage corresponding to zero absorbance was set using water in the observation cell (with a 1-cm path length).

During multiple substrate turnover and ligand binding, changes in the enzyme tryptophan fluorescence were measured with excitation at 280 nm and detection above 305 nm, using a 305 nm cut-off filter. For the fluorescence experiments, the photomultiplier voltage was set at 80% of the full scale with the enzyme at the working concentration in buffer and a path length of 0.2 cm.

Single turnover experiments (excess of enzyme over substrate) were analyzed by stopped flow fluorescence using the fluorescent substrate 2-aminopurine riboside. Changes in the substrate fluorescence during substrate turnover were measured with excitation at 312 nm and detection above 335 nm. The photomultiplier voltage was set at 80% of the full scale with the substrate at the working concentration in buffer and a path length of 0.2 cm.

Rapid Quench Analysis—Rapid quench measurements were performed to follow the formation of guanine from guanosine by the 3G*Tv*NH mutant at room temperature and pH 7.0 using a KinTek RQF-3 quenched flow apparatus. The excess of guanosine (1 mM) was mixed with 3G*Tv*NH (50 μM) for various reaction times and quenched with acid (0.4 M HCl). Control samples of guanosine mixed with quencher were also collected and treated the same as the other samples. Samples were kept on ice and filtered at 4 °C using wetted Microcon centrifugal device microconcentrators (YM-30, regenerated cellulose, 30-kDa cut-off; Amicon). The amount of guanine was quantified using reverse phase high pressure liquid chromatography, as described previously (5). The guanine concentration was calculated from a guanine standard curve using the following equation,

$$[\text{guanine}] = \left(\frac{\text{Area}_G - \text{Area}_C}{\text{slope}}\right) \times \text{DF} \qquad \text{(Eq. 1)}$$

where Area_G represents the area of the guanine peak in the reaction sample, Area_C is the area of the guanine peak in the control sample, slope is the gradient of the guanine standard curve (units of area per micromolar guanine), and DF is the dilution factor.

Pre-steady State Data Analysis—Linear and nonlinear curve fittings to progress curves were performed using Microsoft Origin version 7. The first 2 ms of the progress curves were discarded. Goodness of fit was estimated by visual inspection of residuals. The fitting functions used have the general form,

$$y(t) = \sum_i A_i \exp(-k_i t) + vt + C \qquad \text{(Eq. 2)}$$

where $y(t)$ represents the observed signal at time t, i is the number of transients in the progress curves, A_i is the amplitude of the ith transient, k_i is the observed rate constant for the ith transient, v is the steady-state velocity, and C is the offset. The fitted parameters were used to make plots of observed rate constants *versus* substrate or ribose concentrations. The concentration dependences of the different observed rate constants were analyzed as described previously (13).

Crystallization, Data Collection, and Processing—Crystals of the 3G*Tv*NH·ImmH complex were grown using the hanging drop vapor diffusion method. A protein solution (9.7 mg/ml) was preincubated with 0.7 mM ImmH and 2 mM dithiothreitol for 1 h at 4 °C. Equal volumes of the protein solution and precipitant solution containing 20% polyethylene glycol 4000 and 0.25 M ammonium sulfate in 10 mM potassium acetate, pH 5.0, were mixed and equilibrated at 20 °C. The crystals were soaked in a cryosolution containing 35% polyethylene glycol 4000, 0.5 M ammonium sulfate, and 30 μM ImmH in 10 mM potassium acetate, pH 5. After several minutes, crystals were transferred to the cryostream (100 K), and data were collected to a resolution of 1.4 Å on beamline X11 (EMBL, Deutsches Elektronen-Synchrotron, Hamburg, Germany). The diffraction data were integrated, scaled, and merged with the HKL package (16). Intensities were converted to structure factors using TRUNCATE (17). Relevant statistics for the data set are summarized in Table 1.

Structure Determination and Refinement—The coordinates of one monomer of the wild-type *Tv*NH (Protein Data Bank code 1HOZ, with all of the ligands and flexible parts removed) were used as a search model to solve the structure of the co-crystallized 3GTvNH·ImmH complex by molecular replacement using the program PHASER (18). The same set of reflections for cross-validation was used. To remove model bias maximally and to fill up the gaps in the model, the solution from the molecular replacement was subjected to 10 rounds of automated model building (WarpNtrace) in ARP/WARP (19). The model from ARP/WARP was checked, corrected, and further built in COOT (20). Several cycles of refinement using REFMAC (21) were alternated with manual rebuilding in σA-weighted ($2F_o - F_c$, ϕc) and ($F_o - F_c$, ϕc) electron density maps using COOT. The maps in both active sites in the asymmetric unit showed unambiguous electron density for the inhibitor. The completed model contains two chains of 317 amino acids, two ImmH molecules (both in alternative conformations), two calcium ions, and 773 water molecules. Relevant statistics for the refinement are given in Table 1. Figures were prepared with Pymol (22).

RESULTS

Proline Scan of the Flexible Loop 2—It had previously been suggested that residues from the flexible loop 2 are involved in LG group activation (6). In this study, all residues in loop 2 have been mutated to alanines. Tyr^{257} and Tyr^{258} have additionally been replaced by phenylalanines. None of these mutants seemed to have a negative effect on catalysis (k_{cat}), but some showed a significant increase in K_m. Remarkably, replacing Arg^{252} with alanine increases the turnover almost 5-fold. The same phenomenon is observed to a lesser extent in the Y257A and Y258F mutants.

In the current study, we extended this analysis and additionally mutated the seven residues that are located in the center of the loop one after the other to proline to further investigate whether the main chain amines of the flexible loop residues make a contribution to catalysis. The steady state kinetic parameters of these mutants with guanosine as a substrate are compared with the corresponding values for the wild type enzyme (wt*Tv*NH). The same trend is observed as for the alanine scan of the flexible loop 2 (Table 2); none of these single site mutants show a drastic effect on the steady state parameters. Interestingly, the R252P mutation again has a positive effect on the catalytic turnover rate of guanosine.

Pre-steady State Analysis of R252A Mutant—Arginine 252 is located at the tip of loop 2 and is translocated into the active site to form an interaction with the substrate upon loop closure (12) (Fig. 2, *A* and *B*). Mutations of this arginine to either alanine or proline are the only loop mutations that have a significant effect on the catalytic turnover rate (6) (increase of k_{cat}). All of this indicates that arginine 252 has a functional role in the catalytic mechanism of *Tv*NH. Because the *Tv*NH exhibits a complex multistep kinetic mechanism with an overall rate-limiting ribose release (23), we also performed a pre-steady state kinetic analysis on the R252A *Tv*NH mutant.

Multiple turnovers of guanosine by R252A *Tv*NH, analyzed by stopped flow absorbance, show a biphasic burst of guanine production similar to wt*Tv*NH (Fig. 3*A*). In the R252A *Tv*NH reaction, a fast chemistry step (*N*-glycosidic bond cleavage) is followed by slower product release. The concentration dependence of the burst rates (data not shown) reveals comparable apparent rates of chemistry (k_2 and k_2' in Scheme 1) for wild type and mutant *Tv*NH. Previously, we have shown that multiple turnovers of purine nucleosides by wt*Tv*NH analyzed by stopped flow fluorescence allow the assignment of transients to substrate binding and base release (13). Progress curves of guanosine hydrolysis by R252A *Tv*NH also consist of two transients that correspond to substrate binding and base release (Fig. 3*B*). The concentration dependences of the observed rate constants (k_1, k_{-1}, and k_3 in Scheme 1) indicate that the R252A mutation has no drastic effects on these processes.

In the next step, ribose binding to the R252A mutant was analyzed by stopped flow fluorescence. The concentration dependence of the observed rates of ribose binding

TABLE 1
Data collection and refinement statistics

Parameters	Values
Diffraction data	
Space group	$P2_1$
A (Å)	54.18
B (Å)	74.88
C (Å)	72.42
β (deg)	98.07
Resolution range (Å)[a]	40–1.4 (1.45–1.4)
R_{sym} (%)[a]	7.2 (60.5)
I/σ[a]	20.36 (2.19)
Completeness (%)	100 (99.8)
Redundancy	4.6 (3.6)
Structure refinement	
R_{cryst} (%)	17.73
R_{free} (%)	20.43
Root mean square deviation for bond lengths (Å)	0.008
Root mean square deviation for bond angles (deg)	1.252
Ramachandran plot (% favoured, allowed, outliers)	98.51, 100, 0
No. of atoms/atomic unit	5668

[a] Values in parentheses are for the highest resolution shell.

TABLE 2
Comparison of steady state kinetic parameters of mutant and wild type *Tv*NH at 25 °C and pH 7.0

*Tv*NH	k_{cat}	K_m	k_{cat}/K_m
	s^{-1}	μM	$M^{-1}\,s^{-1}$
Guanosine			
Wild type	2.3 ± 0.1	2.3 ± 0.5	(1.0 ± 0.2) × 10^6
H247P	4.1 ± 0.4	8 ± 3	(5 ± 2) × 10^5
C248P	1.09 ± 0.06	4 ± 1	(2.7 ± 0.7) × 10^5
E249P	1.7 ± 0.1	3 ± 1	(4 ± 1) × 10^5
L250P	1.4 ± 0.1	16 ± 4	(8 ± 2) × 10^4
L251P	2.5 ± 0.1	21 ± 4	(1.2 ± 0.2) × 10^5
R252P	13 ± 1	24 ± 6	(5 ± 1) × 10^5
D253P	3.9 ± 0.2	1.8 ± 0.6	(2.2 ± 0.7) × 10^6
3G	1.52 ± 0.09	266 ± 60	(6 ± 1) × 10^3
2-Aminopurine riboside			
Wild type	0.57 ± 0.03	9 ± 3	(6 ± 2) × 10^5
3G	0.22 ± 003	30 ± 15	(7 ± 4) × 10^4
7-Methylguanosine			
Wild type	1.07 ± 0.02	0.5 ± 0.1	(2.1 ± 0.4) × 10^7
3G	56 ± 2	15 ± 2	(3.7 ± 0.5) × 10^7

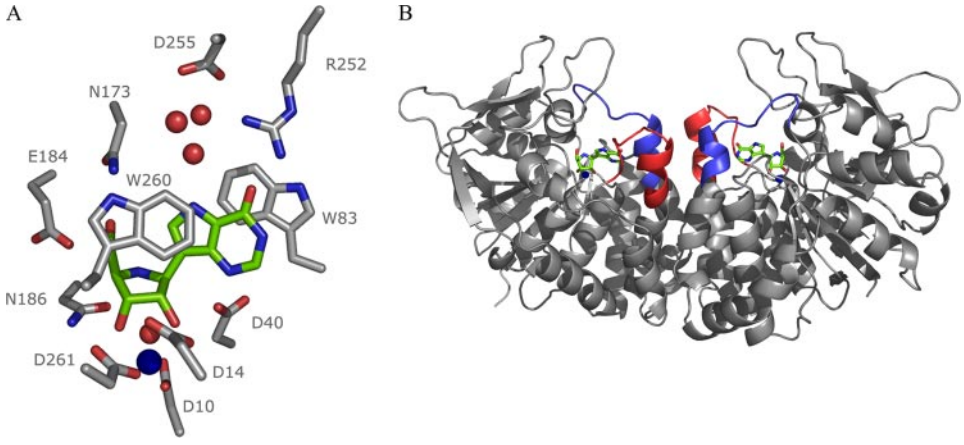

FIGURE 2. *A*, active site of the closed structure of wild type *Tv*NH in complex with the transition state inhibitor ImmH (Protein Data Bank entry 2FF2). The Arg^{252} and Asp^{255} are provided by loop 2. The bound inhibitor, ImmH, is shown in *green*. The Ca^{2+} and water molecules are represented as *blue* and *red spheres*, respectively. *B*, quaternary structure of the closed structure of wild type *Tv*NH in complex with ImmH (Protein Data Bank entry 2FF2). Loop 1 is shown in *blue*, and loop 2 is *red*. The ImmH is represented as a *green ball and stick* model.

shows that this process occurs via the same two-step binding mechanism as seen for the wild type enzyme (23). This two-step binding mechanism consists of a first collision step (K_{ribose} in Scheme 1) to form a loosely bound enzyme ribose complex, followed by an isomerization that converts this loosely bound complex into a tightly bound complex (k_4 and k_{-4} in Scheme 1). In the reverse direction, this isomerization is very slow (k_4) and is the overall rate-determining step for purine hydrolysis catalyzed by wt*Tv*NH. The rate of this isomerization (k_4) is increased from 0.06 s^{-1} for the wild type enzyme to 2.7 s^{-1} for the R252A mutant. The rate of ribose release is identical to the steady state turnover rate of guanosine and hence determines the steady state rate of the R252A mutant.

To summarize, the increase in the catalytic turnover of guanosine by the R252A mutant compared with wt*Tv*NH results from a faster ribose release in the mutant. In the process of ribose release of the R252A *Tv*NH-catalyzed reaction, the isomerization (k_4) prior to ribose dissociation, however, remains the overall rate-limiting step (Table 3).

Loop Deletion—The possible role of loop 2 in the mechanism of *Tv*NH cannot be perturbed by single site mutagenesis, probed by the alanine and proline scan. To assess whether loop 2 as a whole has a more "global" role in the mechanism, we generated a loop deletion mutant, 3G*Tv*NH, where all 13 residues of loop 2 (between Met^{244} and Tyr^{258}) are replaced by three glycine residues. High expression levels of the protein and a single peak on the chromatogram of a high resolution gel filtration pointed out that the 3G*Tv*NH is a stable dimeric protein.

To probe the contribution of the entire loop to catalysis, we compared the kinetic parameters of 3G*Tv*NH and wild type *Tv*NH for three different substrates: 1) guanosine, the genuine substrate of the wild type enzyme; 2) 2-aminopurine riboside (2apr), a fluorescent guanosine analogue that follows the same kinetic model as guanosine for wt*Tv*NH; and 3) 7-methylguanosine, (7mguo) a guanosine analogue with an activated (positively charged) purine ring that needs no further leaving group activation by enzymatic protonation. We have previously shown that 7mguo can be used to quantify the fraction of the catalytic contribution due to leaving group activation (10).

Deletion of loop 2 results in only minor changes in the steady state kinetic parameters for the three substrates tested (Table 2).

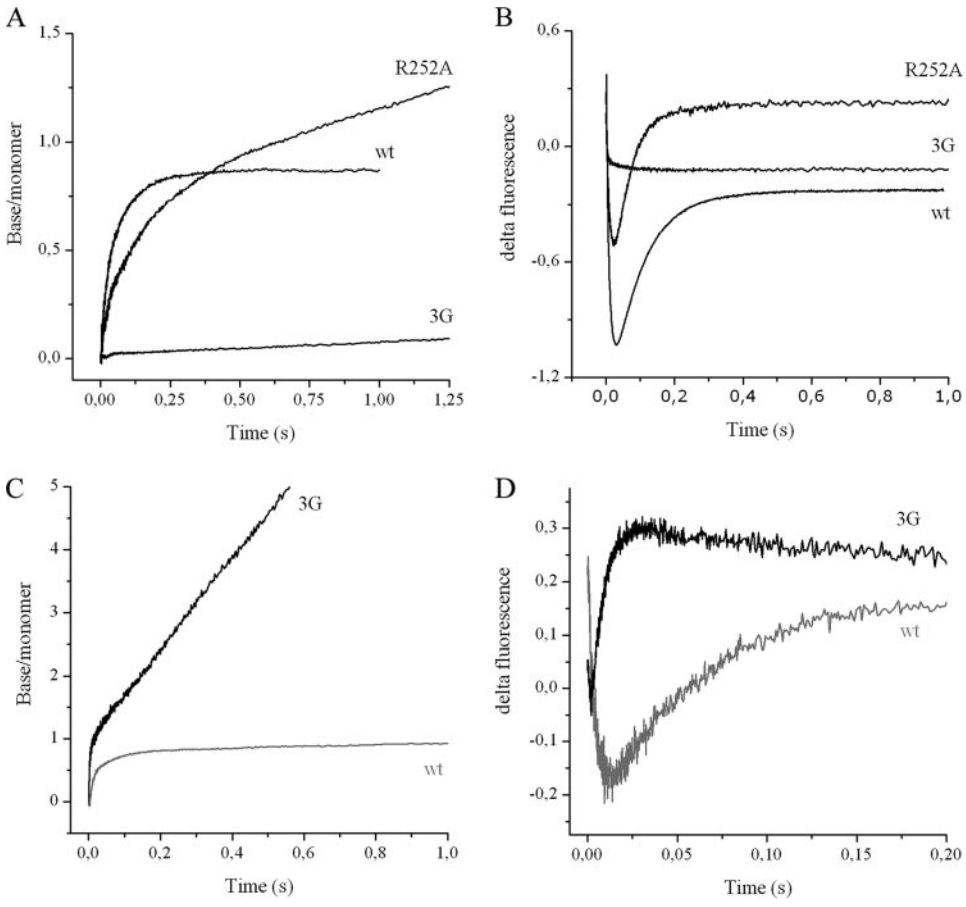

FIGURE 3. **Comparison of multiple turnovers of guanosine (*A* and *B*) and 7mguo (*C* and *D*) by mutant (R252A and 3G) and wild type *Tv*NH analyzed by absorption and fluorescence spectroscopy.** A final concentration of 5 μM enzyme for the absorption experiments (*A* and *C*) and 2 μM enzyme for the fluorescence experiments (*B* and *D*) was mixed with various concentrations of substrate (25–100 μM). The traces shown here represent the turnover of 75 μM substrate.

TABLE 3

Comparison of pre-steady state kinetic parameters of mutant and wild type *Tv*NH at 5 °C and pH 7.0

The rate constants of the rate determining step are shown in bold.

*Tv*NH substrate	Substrate binding				Chemistry		Base release	Ribose release		
	k_1	k_{-1}	k_1'	k_{-1}'	k_2	k_2'	k_3	k_4	k_{-4}	K_D
	$\mu M^{-1} s^{-1}$	s^{-1}	$\mu M^{-1} s^{-1}$	s^{-1}	s^{-1}	s^{-1}	s^{-1}	s^{-1}	s^{-1}	mM
Wild type guanosine[a]	1.24	26	NO[b]	NO	82	8.5	25	**0.06**	21	67
Wild type 7mguo	2.1	46	NO	NO	240	15	20	**0.06**	21	67
R252A guanosine	0.72	25	NO	NO	100	6.5	25	**2.76**	26	75
3G guanosine	1.8	73	0.1	5	**0.06**	NO	NO	6.2	21	38
3G 7mguo	Too fast	Too fast	NO	NO	>300	NO	>200	**6.2**	21	38

[a] Data taken from Ref. 13.
[b] NO, not observed.

3G*Tv*NH hydrolyzes guanosine and 2apr with a turnover comparable with that of the wild type, but an increase in K_m is observed for both substrates. 7Mguo is hydrolyzed even faster by 3G*Tv*NH compared with the wild type, and hardly any difference is observed in the K_m. Consequently, the steady state turnover rate of the 3G*Tv*NH mutant is 50 times higher for 7mguo than for guanosine and 2apr.

In addition, we determined the inhibition constant for the transition state inhibitor ImmH. The inhibition constant is 19 μM, which is 3 orders of magnitude inferior than observed for the wt*Tv*NH (6.2 nM).

Pre-steady State Analysis of 3GTvNH—The catalytic turnover rate of purine nucleosides by wt*Tv*NH is determined by the rate of ribose release. As a result, the steady state rate of hydrolysis is comparable for the three substrates used. Interestingly, the steady state rate of hydrolysis of these substrates differs for the 3G*Tv*NH. To determine the effect of the loop deletion on the individual steps of the kinetic model, we embarked on a detailed pre-steady state kinetic analysis of 3G*Tv*NH using these three substrates.

Shift in Rate-limiting Step of Guanosine and 2apr Hydrolysis—Multiple turnovers of guanosine and 2apr by 3G*Tv*NH analyzed by stopped flow absorbance do not follow burst kinetics (Fig. 3*A*). This implies that product release is not the rate-limiting step for this mutant. This was confirmed by quenched flow analysis. No guanine burst is observed during multiple turnovers of guanosine analyzed by quenched flow (data not shown). Hence, the rate-limiting step of the hydrolysis of guanosine and 2apr catalyzed by 3G*Tv*NH occurs before the chemistry step or is the chemistry step (k_2 in Scheme 1) itself.

Fast Chemistry Step during 7mguo Hydrolysis—Multiple turnovers of 7mguo analyzed by stopped flow absorbance do follow burst kinetics (Fig. 3*C*). Hydrolysis of this activated substrate thus consists of a fast chemistry step (k_2) followed by a rate-limiting product release. Only a single burst transient is observed, and the amplitude corresponds to full site activity. During turnover by the wt*Tv*NH, two transients that include chemistry are observed in the burst. The biphasic burst indicates the existence of two enzyme-substrate complexes in the wild type enzyme. In contrast, only one transient that includes chemistry is observed during turnover catalyzed by 3G*Tv*NH. This implies that for 3G*Tv*NH either only one enzyme substrate complex is formed, or conversion between the two enzyme-substrate complexes is very fast. The dependence of the burst rate on the 7mguo concentration shows some saturation behavior, but not sufficient to determine the maximal burst rate (k_2). A lower bound of 300 s^{-1} (Table 3) can be set for the burst rate, which is very comparable with the fastest burst rate for wt*Tv*NH (240 s^{-1}).

Fast Substrate Binding, Fast 7-Methyl Guanine Release—In a next step, we analyzed multiple turnovers of these substrates with stopped flow fluorescence. For guanosine hydrolysis by 3G*Tv*NH, two transients that correspond to substrate binding were measured, but no transients corresponding to base release were observed (Fig. 3*B*). The observation of (fast) substrate binding (with corresponding rate constants k_1, k_{-1}, k_1', and k_{-1}' in Scheme 1 and Table 3) excludes the possibility that substrate binding is a rate-limiting process for guanosine hydrolysis. We observed no base release transient, confirming that the rate-limiting step occurs before product release. On the contrary, the fluorescence progress curves of 7mguo hydrolysis (Fig. 3*D*) contain transients corresponding to very fast substrate binding and base release, which allowed us to determine the corresponding rate constants (k_1, k_{-1}, and k_3 in Scheme 1 and Table 3).

A Faster Ribose Release Is the Overall Rate-limiting Step of 7mguo Hydrolysis—The observation of a fast base release (k_3) for 7mguo hydrolysis by 3G*Tv*NH indicates that the release of ribose is the overall rate-limiting step for this substrate analogue. To confirm this, we analyzed ribose binding to 3G*Tv*NH by stopped flow fluorescence. Like in wild type enzyme, ribose binds via a two-step binding mechanism. Notably, the rate of release of ribose from 3G*Tv*NH is increased by 2 orders of magnitude compared with the wild type enzyme (k_4 in Scheme 1 and Table 3). In conclusion, deletion of the loop thus results in a faster ribose release. The rate of the isomerization from tightly bound to loosely bound ribose (k_4, 6.2 s^{-1}) is identical to the steady state rate of 7mguo hydrolysis (7 s^{-1} at 5 °C) and hence is the overall rate-limiting step during 7mguo turnover. The rate of ribose release from 3G*Tv*NH is significantly faster than the steady state rate of guanosine and 2apr hydrolysis, which confirms that ribose release cannot be the rate-limiting step of turnover of these substrates.

Chemistry Is the Overall Rate-limiting Step for Guanosine and 2apr Hydrolysis—In a final pre-steady state experiment, single turnovers of 2apr were analyzed by stopped flow fluorescence using the fluorescent properties of 2apr. We compared the single turnover transients of 2apr hydrolysis catalyzed by 3G*Tv*NH with those catalyzed by wt*Tv*NH. Both progress curves consist of two phases with opposite amplitudes (data not shown). Based on the concentration dependence of the rates of the transients, the first phase can be assigned to substrate binding for both progress curves. The second phase of the wt*Tv*NH progress curve consists of two transients that correspond to chemistry and base release. The second phase of the 3G*Tv*NH progress curve is very slow, and the rate of this transient at substrate saturation (estimated at 0.08 s^{-1}) approximates the steady state rate of hydrolysis of 2apr by 3G*Tv*NH (0.05 s^{-1} at 5 °C). The lack of burst kinetics for 2apr and guanosine hydrolysis in combination with these single turnover experiments strongly suggest that the chemistry step (k_2 in Scheme 1 and Table 3) itself is the rate-limiting step of turnover of 2apr and guanosine by 3G*Tv*NH.

Solvent Isotope Effects—In order to attain some corroborating evidence for the shift in the rate-limiting step observed during the pre-steady state analysis, we examined the effects of deuterium oxide on the steady state kinetics of guanosine turnover by wild type *Tv*NH and 3G*Tv*NH at 25 °C (Fig. 4). These measurements demonstrate a small normal solvent isotope effect of 1.3 on the steady state turnover rate k_{cat} for hydrolysis catalyzed by wt*Tv*NH (Fig. 4*A*) and a large normal solvent isotope effect of 2.1 on k_{cat} for hydrolysis catalyzed by 3G*Tv*NH (Fig. 4*B*). No effects were observed on the Michaelis-Menten constant K_m of either enzyme. The difference in the solvent isotope effect between the wild type and the loop deletion mutant confirms that deletion of loop 2 results in a shift of the

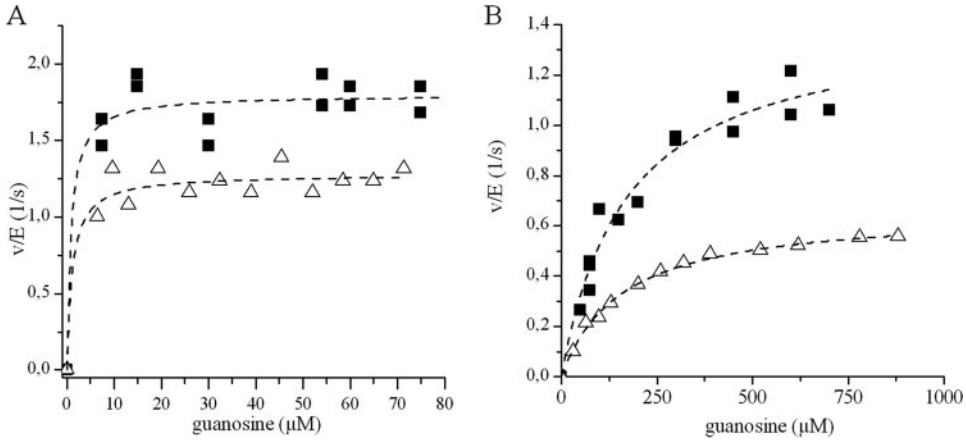

FIGURE 4. **Comparison of solvent isotope effects on steady state parameters of guanosine turnover by wild type and the deletion mutant of *Tv*NH at 25 °C and pL = 7.** The *filled squares* represent the data of the measurements in H_2O, whereas the *open triangles* represent the data of measurements in D_2O. *A*, solvent isotope measurements on the guanosine turnover by wild type *Tv*NH. *B*, solvent isotope measurements on the guanosine turnover by 3G*Tv*NH. The *dotted lines* represent the fits to the Michaelis-Menten equation.

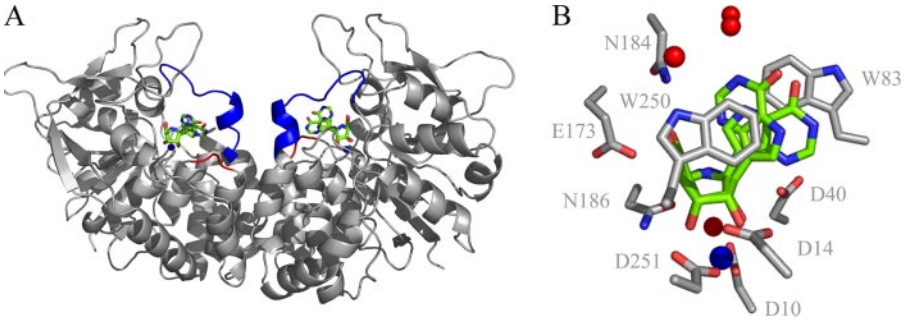

FIGURE 5. *A*, quaternary structure of the loop deletion mutant in complex with the transition state inhibitor ImmH. Loop 1 is shown in *blue*, and the three glycines that replace the 13 loop 2 residues are shown in *red*. The inhibitor is shown in *green*, and the Ca^{2+} is represented as a *blue sphere*. *B*, active site of the loop deletion mutant. The bound inhibitor, ImmH, is shown as a *green ball and stick model*. The Ca^{2+} and water molecules are represented as *blue* and *red spheres*, respectively.

overall rate-limiting step of the hydrolysis reaction. The solvent isotope effect on k_{cat} of the loop deletion mutant is even bigger than the previously observed solvent isotope effect on the chemistry transient of the wild type enzyme (1.68) (15).

Role of Loop 2 in LG Activation—Taken together, this pre-steady state analysis and the solvent isotope effects demonstrate that the kinetics of the hydrolysis of guanosine (and also 2apr) by 3G*Tv*NH and wt*Tv*NH are characterized by different rate-limiting processes. Although the isomerization prior to ribose dissociation (k_4) is rate-limiting for wt*Tv*NH, chemistry (k_2) becomes rate-limiting for 3G*Tv*NH. The deletion of the flexible loop thus results in a decrease of 3 orders of magnitude of the apparent rate of chemistry for these two substrates (k_2, 82 s^{-1} in wt*Tv*NH to 0.06 s^{-1} in 3G*Tv*NH). In contrast, the rate-limiting step for the hydrolysis of the "activated" substrate 7mguo is the same slow isomerization prior to ribose dissociation (k_4) in 3G*Tv*NH as in wild type enzyme. Thus, chemistry (k_2) is hardly affected by the loop deletion for the activated substrate. Taken together, this observed difference in the kinetic effect of the loop deletion on hydrolysis of a genuine substrate as compared with the activated substrate reveals a substantial role of loop 2 in LG activation.

Loop Deletion Is a Nondestructive Mutation—To investigate the effects of loop deletion on the structural integrity of the protein, we also solved the x-ray structure of 3G*Tv*NH in complex with the transition state inhibitor ImmH. This structure was refined to 1.4 Å resolution, yielding a final *R*-factor of 17.73% (R_{free} = 20.43%). The crystal contains a homodimer in the asymmetric unit, and both active sites are fully occupied with ImmH. Both subunits show the characteristic α/β nucleoside hydrolase fold (2). Loop 2 is nicely bypassed by the three incorporated glycine residues in both subunits (Fig. 5*A*). The residues flanking these glycine residues (methionine 244 and tyrosine 248 in the 3G*Tv*NH numbering) superpose perfectly with the corresponding residues of the wild type complex with ImmH. The rest of the protein backbone is mainly unaffected by the loop deletion, with an average root mean square deviation of 0.4 Å between all main chain atoms of a 3G*Tv*NH·ImmH and a wt*Tv*NH·ImmH subunit (Protein Data Bank code 2FF2). Besides loop 2, which has been deleted, the 3G*Tv*NH·ImmH complex shows all of the characteristics of a closed conformation, similar to the wt*Tv*NH·ImmH co-crystallized complex (12). Loop 1 is completely fixed (Fig. 4*A*) with *B*-factors comparable with the mean value for the entire protein. Trp^{242} and Asp^{14}, the two residues that were suggested to be involved in the trigger mechanism of loop closure, are in their "closed" conformation. All other active site residues are also in the same position as in the wild type complex (Fig. 5*B*). In both active sites, ImmH is bound in two alternative conformations, namely the *anti* and *syn* conformations, which corresponds to a glycosidic torsion angle χ (N4′–C1′–C9–C4) close to 180° and 0°, respectively. In the wild type complex, the ImmH was observed only in the *anti* conformation. However, the *syn* conformation has been observed in the complex of wt*Tv*NH with the inhibitor 3-deaza adenosine (6). The iminoribitol moieties of all of the ImmH molecules bound to 3G*Tv*NH adopt a *C′4-endo* conformation, corresponding to a pseudorotation angle of about 230°, as observed in the wild type complex. The channel of water molecules that connects N-7 of the leaving group of the inhibitor with bulk solvent is also observed in the active sites of the 3G*Tv*NH·ImmH complex. Only the water molecule hydrogen-bonded to N-7 is missing. This is probably due to the occurrence of the *syn* conformation of the bound inhibitor, which makes it impossible for the water molecule to take in this position.

Based on this high resolution structure, we can conclude that the deletion of loop 2 has no drastic effects on the global fold of

the protein or on the active site catalytic interactions. Therefore, the observed kinetic effects can be confidently attributed to the lack of loop 2 *per se*.

DISCUSSION

Flexible loops are protein structural elements often found near the binding sites or active sites of receptors and enzymes. Binding of ligands is often accompanied by an open-to-closed or disordered to ordered conformational change of these flexible loops. The loops presumably play an important role in gating ligand association and dissociation and altering the reaction environment markedly by closing over the active site. Moreover, the closed active site can prevent solvolysis of the reaction intermediates and discriminate between the ground state and the transition state (24).

Flexible active site loops are also a common feature of the nucleoside hydrolases (2). All structures of the nucleoside hydrolases determined until now show two flexible loops in the vicinity of the active sites, called loop 1 and 2, which undergo substantial conformational changes upon association of substrates and inhibitors (12, 25–27). We recently published the structure of the co-crystallized wt*Tv*NH·ImmH complex, confirming the ordering of both loops and the folding of loop 2 over the active site upon transition state binding (12). Moreover, the ordered loop 1 of one subunit of the homodimer interacts with the ordered loop 2 of the other subunit, and *vice versa*.

A Catalytic Role of Loop 2 in Leaving Group Activation—In this study, we used a combination of single site mutagenesis, loop deletion mutagenesis, steady state and pre-steady state kinetics, and x-ray crystallography to probe the role of the flexible loop 2. Comparison of the kinetics of purine nucleoside hydrolysis reveals that deletion of loop 2 results in a shift of the overall rate-limiting step from ribose release for the wild type enzyme to chemistry for the deletion mutant. This shift results from an increase in the rate the isomerization prior to ribose dissociation (k_4 in Scheme 1) concomitant with a decrease in the rate of chemistry (k_2 in Scheme 1) by 3 orders of magnitude. Coincidentally, the resulting rate of chemistry is very comparable with the rate-limiting ribose release during purine turnover by wt*Tv*NH, which explains the apparent unaffected steady state turnover rate. The shift in overall rate-limiting step as a result of loop deletion is supported by the difference in solvent isotope effects between the hydrolysis catalyzed by wild type and mutant enzyme. A large solvent isotope effect (2.1) was observed on the steady state turnover rate catalyzed by the deletion mutant, whereas only a small effect (1.3) was observed during turnover catalyzed by the wild type enzyme. These solvent isotope effect measurements confirm our conclusion that the deletion of the flexible loop shifts the rate-limiting step from product release to chemistry, since an increase in solvent isotope effect is observed. However, the exact nature of the observed solvent isotope effects is still uncertain and requires an elaborate study. Nevertheless, a normal solvent isotope effect of 2 is within the range observed for solvation catalytic bridges between oxygen and nitrogen, which would imply a concerted proton transfer of a proton from solvent to the leaving group.

Hence, loop deletion leads to a hampered catalysis of the hydrolysis of the *N*-glycosidic bond. The catalytic role involves a "global" effect of the entire loop, which could not be perturbed by single site mutagenesis. The steady state kinetic characterization of the single mutants generated by an alanine scan (6) and also a proline scan (this study) of the loop residues shows that there are no individual catalytically important interactions with the substrate that can be attributed to a single loop residue side chain or main chain amide. The pre-steady state analysis of the single site mutant R252A moreover proves that deletion of the arginine side chain does not affect the rate of chemistry (k_2). Although we have investigated only one of the single site mutants in detail by pre-steady state analysis, the unchanged k_{cat}/K_m values for the different mutants compared with the one of wild type enzyme indicate that the rate of chemistry is unaffected by the single site mutations.

The loss in catalytic efficiency caused by the deletion of the entire loop is not observed during turnover of 7mguo. The rate of chemistry (k_2) of 7mguo turnover by the deletion mutant is comparable with that of wild type enzyme. 7mguo is a guanosine analogue with an activated (positively charged) purine ring and needs no further activation by enzymatic protonation for expulsion. Because the catalytic contribution of loop 2 is only observed in substrates where the leaving group is not *a priori* activated, its catalytic role can be pinpointed at the level of leaving group activation. Most probably, the loop contributes to the protonation of the substrate's N-7 by solvent. A thermodynamic cycle at the level of the chemical step (k_2; Scheme 1 and Table 3), calculating the energetic coupling between the loop deletion (wild-type *versus* 3G*Tv*NH) and the methylation/quaternization of N-7 (guanosine *versus* 7mguo), shows that the magnitude of this catalytic effect amounts to 4.11 kcal/mol.

Activation of the leaving group by N-7 protonation results from aromatic stacking of the leaving group with Trp^{260} and an intramolecular O5′–HC8 hydrogen bond formation, which can raise the pK_a of a purine nucleobase sufficiently to promote direct protonation by solvent (10, 11). Closure of loop 2 of *Tv*NH can contribute to N-7 protonation by squeezing out most of the water to retain a few selected water molecules that form the observed network of highly ordered water molecules to connect the substrate with bulk solvent. This network may act as a proton relay system shuttling protons directly to the high pK_a N-7 of the substrate. Furthermore, the water channel is lined by residues of the ordered loop 2, which can aid the channel to act as a proton relay system.

This proposal is in accordance with the generally accepted view that loop closures separate the bulk water from the reaction region (24, 29, 30). In such models, water is either squeezed out of the active site, or a limited number of selected water molecules are retained for catalysis. This effectively creates a low dielectric medium where electrostatic interactions are enhanced (24). It has been shown that the stabilization of polar transition states occurs better in the active site of enzymes than in water (32). The active sites of enzymes can provide higher solvation energy than an aqueous solution. The dipoles of the first few solvation shells of bulk water cannot be strongly polarized toward the charges, because they interact with the sur-

rounding randomly oriented bulk dipoles. Small clusters of organized water molecules in active sites do not experience this depolarization by the surrounding water shells. This means that a closed active site allows enzymes to stabilize charges by their own dipoles in combination with a few water molecules, which leads to a better stabilization of the transition state than achieved in bulk solvent (33).

Loop Dynamics Determine Substrate Binding and Product Release—After the hydrolysis of the *N*-glycosidic bond of purine nucleosides by the wild type *Tv*NH, the ordered release of both products involves four steps. Prior to dissociation of each product from the enzyme (K_{base} for base and K_{ribose} for ribose in Scheme 1), the enzyme product complexes undergo a slow isomerization from a tightly bound to a loosely bound enzyme product complex (k_3 for base and k_4 for ribose in Scheme 1) (13). The isomerization prior to ribose dissociation (k_4) is the overall rate-limiting step during substrate turnover by wt*Tv*NH. This isomerization is the only process that is affected by the single site mutation of Arg^{252} to alanine. The deletion of the arginine side chain increases the isomerization rate prior to ribose (k_4) dissociation 50-fold. Nevertheless, this step remains the overall rate-limiting step during substrate turnover in the mutant. The deletion of loop 2 results into a faster release of the base (k_3, based on 7mguo hydrolysis analyzed by fluorescence) and a faster release of the ribose (k_4, based on ribose binding analyzed by fluorescence) during purine nucleoside turnover. Without the loop, the base is released 10 times faster; ribose is released even 100 times faster, as a result of a faster isomerization prior to product dissociation (k_3 and k_4 for base and ribose release, respectively).

All of these kinetic data indicate that loop movements are implicated in the isomerizations prior to product dissociation. X-ray crystallographic data also indicate that loop movements play a key role in product release. The structure of the wild type *Tv*NH·ImmH complex shows that during chemistry, the N-terminal part of loop 2 adopts a helical secondary structure, whereas the C-terminal part forms a coil that closes over the active site and brings several residues into the active site. Moreover, the ordered loop 2 interacts with the ordered loop 1 of the other subunit within the homodimer and *vice versa* (12). Turning this around, the helical part of loop 2 needs to relax, whereas the rest of the loop needs to move away from the active site, before the products can dissociate from the enzyme. Unfolding of the helical part of loop 2 will also disrupt the interaction with loop 1 of the neighboring subunit. The relaxation of the helix, with concomitant disruption of the interaction with loop 1 and the opening of the active site, most probably relates to the slow isomerization steps prior to product dissociation (k_3 and k_4 for base and ribose release, respectively), thus limiting the rate of product release. The isomerization required for base release (k_3) occurs faster then the isomerization allowing ribose release (k_4), implying that both isomerizations are different in nature. Probably, the release of base only involves a peripheral opening of the active site consisting of a movement of the active site tryptophans (Trp^{83} and Trp^{260}) away from the base part and opening of the coil part of loop 2. The crystal structure of the wt*Tv*NH·ImmH complex shows that the closure of loop 2 brings the active site Trp^{260} 0.6 Å closer to the leaving group, thus strengthening the aromatic stacking interactions between both heterocyclic systems. Reciprocally, opening of this peripheral lid may allow the base to defuse from the active site. Ribose binds deeper into the cleft and interacts via its 2′-OH to Asp^{14}. The formation of this interaction between ribose and Asp^{14} leads to a torsional flip of the Trp^{242} side chain. This cascade of interactions has been proposed previously to trigger loop ordering and closure over the active site (12). The relaxation of the helical part of loop 2 and the concomitant disruption of the interaction with the loop 1 of the other subunit could lead to the disruption of this interaction and consequent ribose dissociation. In conclusion, ribose release involves a "total" opening of the active site, which occurs much more slowly than the "local" opening prior to base dissociation.

Similar roles for flexible loops in slow, two-step product releases have been described for the hydrolysis reaction of the purine nucleoside phosphorylase (34). For this enzyme it was demonstrated that binding of substrate causes an active site loop to be converted to a helix that blocks the release of product. Relaxation of the helix limits the rate of product release.

Obviously, the fluorescence signals coupled to ribose and base release do not stem directly from loop closure, since similar fluorescence transients of this isomerization are observed when the loop is deleted. However, base release involves Trp^{260} moving away from the base. This process can easily explain the large fluorescence signal coupled to the peripheral isomerization and base release. Possibly, it is the torsional flip of the Trp^{242} side chain, coupled to the interaction of ribose with Asp^{14}, that causes changes in fluorescence intensities associated with the complete opening of the active site followed by ribose dissociation. Although the loop is deleted in the 3G*Tv*NH enzyme, the interactions of 2′-OH with Asp^{14} still cause the flipping of the Trp^{242} in the 3GTvNH·ImmH x-ray structure.

Loop 2 Limits the Interconversion Rate of the Syn to Anti Conformation—The biphasic burst kinetics observed during purine nucleoside turnover by wild type *Tv*NH implies that two different and interconverting enzyme-substrate complexes are formed (13). Possibly, only one of both complexes is catalytically competent to undergo chemistry (Scheme 1). The other complex needs to convert to the catalytic active one before chemistry can take place. The fast phase of the burst thus corresponds to the catalytically competent complex that undergoes chemistry (k_2 in Scheme 1). The rate of the slow phase corresponds to the conversion rate of the inactive to the catalytic active enzyme-substrate complex (k_2' in Scheme 1) followed by chemistry. It was previously suggested that the two enzyme-substrate complexes differ in the conformation of the bound substrate. One complex could contain the nucleoside in the *syn* conformation, whereas the other complex has the nucleoside bound in the reactive *anti* conformation. Both conformations have been observed previously by crystallography. The *anti* conformation is the most common conformation and was observed in the wt*Tv*NH·ImmH cocrystallized complex (12). The *syn* conformation was only observed for the wt*Tv*NH 3-deaza-adenosine complex (5). Furthermore, turnover of inosine in the *anti* conformation was observed in the crystal structure of the slow D10A mutant soaked with the substrate

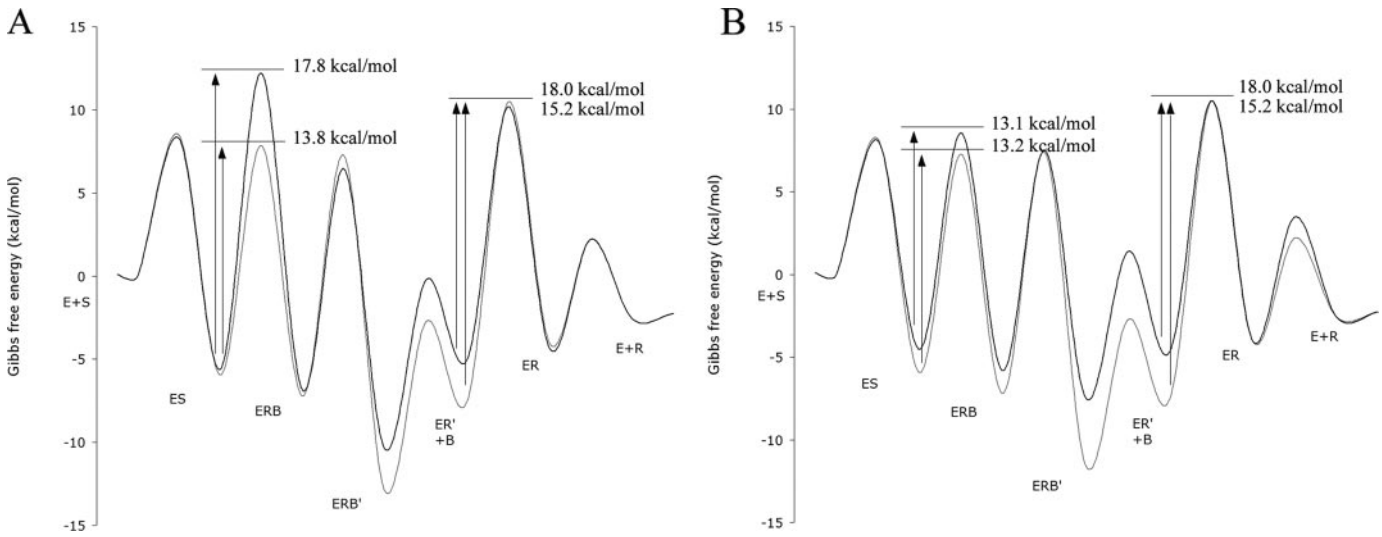

FIGURE 6. **Comparison of energy profiles of guanosine (*A*) and 7-methylguanosine (*B*) turnover catalyzed by the deletion mutant (*black curve*) and the wild type *Tv*NH (*gray curve*).** For clarity of the figure, the formation of the second enzyme substrate complex (*E*·S′) was excluded from the graph. The energy barrier for each reaction step was calculated using the equation, $\Delta G^{\neq} = -RT(\ln(k_i) - \ln(k_b T/h))$, where R represents the gas constant, T is the absolute temperature, k_b is the Boltzman constant, h is the Planck constant, and k_i is the rate constant of the reaction step. The magnitudes of the energy barriers of chemistry and the isomerization prior to ribose release are indicated. Substrate concentrations were taken at unity, and the product concentrations were calculated based the equilibrium constant of 106 M between nucleoside and base (28). The $E + S$ state was taken as the reference state, and based on the equilibrium constant of 106 M, we were able to calculate the free energy of the $E + R$ state. The association constant rates for base and ribose were assumed to be of the typical order of $10^8\ M^{-1}\ s^{-1}$ (31). Based on the fact that the burst amplitude of base formation equals more then 90%, we can state that the rate of the reverse chemistry step must be equal to or less than 10% of the forward chemistry rate.

inosine, indicating that the *anti* conformation is a catalytically competent conformation (6). This could imply that the substrate bound in the *syn* conformation needs to convert to the *anti* conformation before chemistry can take place. Considering the size of a purine base, loop 2 most probably needs to move away from the active site for this conversion to occur. For free nucleosides, interconversion between the two conformers takes place on the nanosecond time scale (35), but the relaxation and opening of the active site will limit the rate of this conversion (k_2'). Consistent with this notion, the bound inhibitor adopts both conformations with comparable occupancies in each active site of the high resolution structure of the 3G*Tv*NH mutant, solved at a resolution of 1.4 Å. This hypothesis is supported by the full-site, single phase burst upon 7mguo hydrolysis by the deletion mutant in pre-steady state. Indeed, a fast interconversion of the two complexes results in a single phase product burst and implies the perception of only a single enzyme substrate species.

Conclusion and Model—On the basis of the results obtained in this study, combined with previous results, we can compare the energy profiles of the hydrolysis catalyzed by wild type enzyme and the loop deletion mutant. From the reaction coordinate of guanosine hydrolysis (Fig. 6*A*), it is easily seen that chemistry (k_2 in Scheme 1) and the isomerization steps prior to the stepwise dissociation of the products (k_3 and k_4 in Scheme 1) are affected by the deletion of the loop. The energy barrier for chemistry (k_2) is increased by 4 kcal/mol, whereas the barrier for the isomerization prior to ribose dissociation (k_4) is lowered by 2.8 kcal/mol. Deletion of loop 2 thus leads to a shift in the rate-limiting step from ribose release to chemistry.

The energy profiles of 7mguo hydrolysis (Fig. 6*B*) show that the energy barrier for chemistry (k_2) is hardly affected by the loop deletion, whereas the energy barrier of the isomerization prior to ribose release (k_4) is lowered by 2.8 kcal/mol by deletion of the loop.

The observation that the loop deletion lowers the chemistry energy barrier for guanosine but not for 7-methyl guanosine, an analog with an activated leaving group, establishes a catalytic role of the loop in leaving group activation. Moreover, the energy profiles clearly show that loop movement is involved in the isomerization prior to product release.

Based on all results presented so far, we can propose the following molecular model. After substrate binding, loop 2 gets ordered. Ordering of loop 2 leads to interactions with loop 1 of the other subunit of the dimer and closes over the active site as a lid. The substrate can bind in two alternative conformations: the *syn* and *anti* conformations. Substrate bound in the *anti* conformation can easily undergo chemistry, whereas substrate bound in the *syn* conformation needs to convert to the *anti* conformation before chemistry can take place. For this conversion to occur, the lid needs to open. After the interconversion of *syn* to *anti*, the lid closes again over the active site. Once the lid is closed, chemistry can take place. Closing loop 2 over the active site contributes to leaving group activation via the formation of a dedicated water channel that shuttles protons from bulk solvent to N-7. After chemistry, the base is released first upon opening of the peripheral lid. Before ribose can dissociate from the active site, a further opening of the active site has to occur. This involves the relaxation of the helical part and disruption of the intersubunit interaction with loop 1.

Acknowledgment—The use of synchrotron beam time at the EMBL (Deutsches Elektronen-Synchrotron, Hamburg, Germany) is acknowledged.

REFERENCES

1. Gutteridge, A., and Thornton, J. (2004) *FEBS Lett.* **567,** 67–73
2. Versees, W., and Steyaert, J. (2003) *Curr. Opin. Struct. Biol.* **13,** 731–738
3. Horenstein, B. A., Parkin, D. W., Estupiñán, B., and Schramm, V. L. (1991) *Biochemistry* **30,** 10788–10795
4. Schramm, V. L. (2003) *Nucleic Acids Res. Suppl.* 107–108
5. Versées, W., Decanniere, K., Pellé, R., Depoorter, J., Brosens, E., Parkin, D. W., and Steyaert, J. (2001) *J. Mol. Biol.* **307,** 1363–1379
6. Versées, W., Decanniere, K., Van Holsbeke, E., Devroede, N., and Steyaert, J. (2002) *J. Biol. Chem.* **277,** 15938–15946
7. Garrett, E. R., and Mehta, P. J. (1972) *J. Am. Chem. Soc.* **94,** 8532–8541
8. Gopaul, D. N., Meyer, S. L., Degano, M., Sacchettini, J. C., and Schramm, V. L. (1996) *Biochemistry* **35,** 5963–5970
9. Mazumder-Shivakumar, D., and Bruice, T. C. (2005) *Biochemistry* **44,** 7805–7817
10. Versees, W., Loverix, S., Vandemeulebroucke, A., Geerlings, P., and Steyaert, J. (2004) *J. Mol. Biol.* **338,** 1–6
11. Loverix, S., Geerlings, P., McNaughton, M., Augustyns, K., Vandemeulebroucke, A., Steyaert, J., and Versees, W. (2005) *J. Biol. Chem.* **280,** 14799–14802
12. Versees, W., Barlow, J., and Steyaert, J. (2006) *J. Mol. Biol.* **359,** 331–346
13. Vandemeulebroucke, A., Versees, W., Steyaert, J., and Barlow, J. N. (2006) *Biochemistry* **45,** 9307–9318
14. Dunn, D. B., and Hall, R. H. (1970) in *CRC Handbook of Biochemistry* (Sober, E. K., ed) CRC Press, Inc., Boca Raton, FL
15. Barlow, J. N., and Steyaert, J. (2007) *Biochim. Biophys. Acta.* **1774,** 1451–1461
16. Otwinowski, Z., and Minor, W. (1997) *Methods Enzymol.* **276,** 307–326
17. French, S., and Wilson, K. (1978) *Acta Crystallogr. Sect. A* **34,** 517–525
18. McCoy, A. J. (2007) *Acta Crystallogr. Sect. D Biol. Crystallogr.* **63,** 32–41
19. Perrakis, A., Harkiolaki, M., Wilson, K. S., and Lamzin, V. S. (2001) *Acta Crystallogr. Sect. D Biol. Crystallogr.* **57,** 1445–1450
20. Emsley, P., and Cowtan, K. (2004) *Acta Crystallogr. Sect. D Biol. Crystallogr.* **60,** 2126–2132
21. Murshudov, G. N., Vagin, A. A., and Dodson, E. J. (1997) *Acta Crystallogr. Sect. D Biol. Crystallogr.* **53,** 240–255
22. DeLano, W. L. (2002) *The PyMOL Molecular Graphics System*, Delano Scientific, San Carlos, CA
23. Vandemeulebroucke, A., Versees, W., De Vos, S., Van Holsbeke, E., and Steyaert, J. (2003) *Biochemistry* **42,** 12902–12908
24. Hammes, G. G. (2002) *Biochemistry* **41,** 8221–8228
25. Giabbai, B., and Degano, M. (2004) *Structure* (*Camb.*) **12,** 739–749
26. Degano, M., Almo, S. C., Sacchetini, J. C., and Schramm, V. L. (1998) *Biochemistry* **37,** 6277–6285
27. Degano, M., Gopaul, D. N., Scapin, G., Schramm, V. L., and Sacchetini, J. C. (1996) *Biochemistry* **35,** 5971–5980
28. Parkin, D. W., Horenstein, B. A., Abdulah, D. R., Estupiñán, B., and Schramm, V. L. (1991) *J. Biol. Chem.* **266,** 20658–20665
29. Chu, V., Freitag, S., Le, T. I., Stenkamp, R. E., and Stayton, P. S. (1998) *Protein Sci.* **7,** 848–859
30. Kempner, E. S. (1993) *FEBS Lett.* **326,** 4–10
31. Eigen, M., and Hammes, G. G. (1963) *Adv. Enzymol. Relat. Areas Mol. Biol.* **25,** 1–38
32. Warshel, A. (1978) *Proc. Natl. Acad. Sci. U. S. A.* **75,** 5250–5254
33. Warshel, A., Sharma, P. K., Kato, M., Xiang, Y., Liu, H., and Olsson, M. H. (2006) *Chem. Rev.* **106,** 3210–3235
34. Kline, P. C., and Schramm, V. L. (1992) *Biochemistry* **31,** 5964–5973
35. Foloppe, N., and Nilsson, L. (2005) *J. Phys. Chem. B* **109,** 9119–9131